

Communication

Ultrawideband and High-Resolution Terahertz Spectroscopy: Structural Identification of Glucose

Katsuhiko Miyamoto ^{1,2,*} , Tomohito Yamasaki ¹, Shota Tsuji ¹, Kazuma Inoue ¹, Godeung Park ¹, Hirohisa Uchida ³ , Akira Matsuura ^{2,4} , Peter Krüger ^{1,2}  and Takashige Omatsu ^{1,2}

¹ Graduate School of Engineering, Chiba University, Yayoi-cho, Inage-ku, Chiba 263-8522, Japan

² Molecular Chirality Research Center, Chiba University, Chiba 263-8522, Japan

³ ARKRAY Inc., Kyoto 602-0008, Japan

⁴ Graduate School of Science, Chiba University, Chiba 263-8522, Japan

* Correspondence: k-miyamoto@faculty.chiba-u.jp

Abstract: We report on the development of an ultrawideband and high-resolution THz spectroscopic system, which operates over a frequency range of 2–13.5 THz. This work goes beyond conventional THz spectroscopic measurements and demonstrates the capacity to differentiate D- and L-glucoses, which have the same molecular conformation and crystal structure. Furthermore, this system facilitates the structural identification of glucose microcrystals, which exists in α - and β -forms, revealing that L-glucose microcrystals are formed of a mixture of α - and β -D-glucose with approximately equal weight.

Keywords: terahertz; spectroscopy; DAST-DFG; density functional theory; glucose



Citation: Miyamoto, K.; Yamasaki, T.; Tsuji, S.; Inoue, K.; Park, G.; Uchida, H.; Matsuura, A.; Krüger, P.; Omatsu, T. Ultrawideband and High-Resolution Terahertz Spectroscopy: Structural Identification of Glucose. *Photonics* **2022**, *9*, 602. <https://doi.org/10.3390/photonics9090602>

Received: 31 July 2022

Accepted: 20 August 2022

Published: 25 August 2022

Publisher's Note: MDPI stays neutral with regard to jurisdictional claims in published maps and institutional affiliations.



Copyright: © 2022 by the authors. Licensee MDPI, Basel, Switzerland. This article is an open access article distributed under the terms and conditions of the Creative Commons Attribution (CC BY) license (<https://creativecommons.org/licenses/by/4.0/>).

1. Introduction

Terahertz (THz) waves [1–9] enable the direct characterization of molecular aggregations and clusters via coupling with vibrational eigenmodes. Thus, this class of electromagnetic waves have the ability to revolutionize applications in fundamental sciences and enable advanced technologies, including structural analysis of crystalline objects [10–14], field-matter interaction [15], nonlinear optical responses [16–18], biological kinetics [19], THz comb spectroscopy [20], quantum sensing [21], scanning probe microscopy [22], coherence tomography [23], and novel imaging methods [24–26].

Fourier transform infrared spectroscopy (FTIR) and THz time-domain spectroscopy (TDS) techniques are well established, and commercial systems based on these techniques have been applied to the identification of molecules, such as nucleosides [27,28], amino acids [29,30], peptides [31], emerging materials [32], and sugars [33–35]. In each of these application cases, the materials under study have exhibited well-defined spectral features in the THz frequency range. Although systems based on THz-FTIR and THz-TDS have seen good commercial success, THz TDS systems, which utilize ultrashort pulse pump lasers, inherently have limited frequency bandwidth for spectroscopic measurements (with the frequency range typically limited to ~0.1–5 THz). FTIR methods enable a wider frequency range, however, they struggle to measure the properties of highly absorbing materials at a high signal-to-noise (S/N) ratio. These approaches also frequently require the use of attenuated total reflection (ATR) and waveguide configurations.

In this paper, we propose a frequency-domain THz spectroscopic system, based on difference frequency generation (DFG), that enables high S/N ratio measurements across a very broad THz frequency range of 2–13.5 THz. We utilize our system for the structural identification of glucose, one of the most prevalent biological molecules in nature.

2. Ultrawideband THz Spectroscopic System

A schematic diagram of the experimental ultrawideband frequency-domain THz spectroscopic system is shown in Figure 1. The frequency-tunable THz source was comprised of a 1 μm homemade picosecond pump source (average power 10 W, pulse width 7.4 ps, pulse repetition frequency 1 MHz), of which an injection seeded two 1.5 μm optical parametric amplifiers (OPAs) [7,36]. The output of the OPAs were then used to generate THz radiation in 4'-dimethylamino-N-methyl-4-stilbazolium tosylate (DAST) crystal via difference frequency generation (DFG). Most of the tunable THz sources are developed by employing a nanosecond laser pumping configuration, and their pulse repetition rates are typically limited to be less than 100 Hz [37–40]. Use of our THz source with an ultrahigh repetition rate of 1 MHz allows the detection with a high signal-to-noise (S/N) ratio and short acquisition time. Frequency tuning of the THz radiation was achieved by fixing the wavelength of the OPA1 output, λ_1 , at 1.50 μm , and tuning the OPA2 output wavelength, λ_2 , in the range 1.50–1.64 μm . The resulting THz output via the DFG process was linearly polarized and could be tuned across the range 2–13.5 THz. The THz output had a linewidth of ~ 0.12 THz at 2.6 THz (wavelength of ~ 116 μm), which is comparable to them of conventional nanosecond THz sources, as measured using a scanning etalon. The THz detection scheme was comprised of a cryogenic Si bolometric detector and a lock-in amplifier, and this enabled the high-resolution detection of the THz radiation with an ultra-high S/N ratio of >50 dB (Figure 1b).

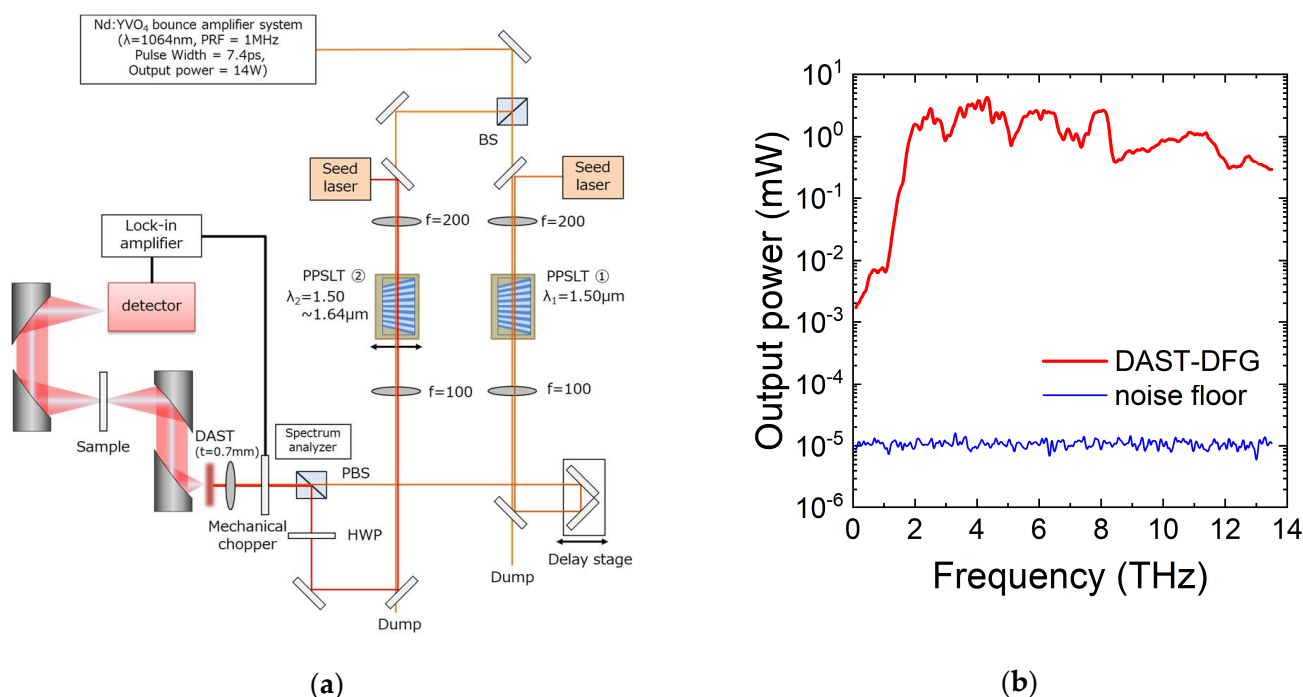


Figure 1. (a) Experimental setup of the frequency-domain THz spectroscopy system based on a tunable THz generator formed using a DAST-DFG. (b) Plot of the average THz output power spectrum and noise floor level of the THz output generated by the DAST-DFG. More than 50 dB of signal to noise ratio can be observed.

3. THz Absorption Spectrum of Glucose Simulated with Density Functional Theory

Glucose ($\text{C}_6\text{H}_{12}\text{O}_6$), the most conventional monosaccharides, belongs to a subcategory of carbohydrates, and it acts as a source of energy, as well as a metabolic intermediary. Glucose with D- and L-enantiomers can further be classified into α and β forms, which arise from the difference in steric position of hydroxy groups to C-1 carbon.

The THz absorption spectra of glucose crystals were numerically computed by employing density functional theory (DFT) with the PBE exchange–correlation potential as

implemented in the VASP code [41,42]. The plane-wave energy cut-off was set to 700 eV, which gave converged results as checked by comparison with a value of 600 eV. Firstly, the crystal structures of α -D-glucose [43] and β -D-glucose [44] were optimized until all atomic forces were below 1 meV/Å. The phonons at the Γ -point, Born effective charges and the infrared spectra were then computed by using density functional perturbation theory [45] (VASP settings IBRION = 7, LEPSILON = T). It is worth mentioning that the computed spectra of single α - and β -D-glucose molecules did not support the experimental data well, manifesting that the intermolecular interactions play an important role for an accurate description of the THz spectra. The computed spectra of α - and β -D-glucose crystals are shown in Figure 2.

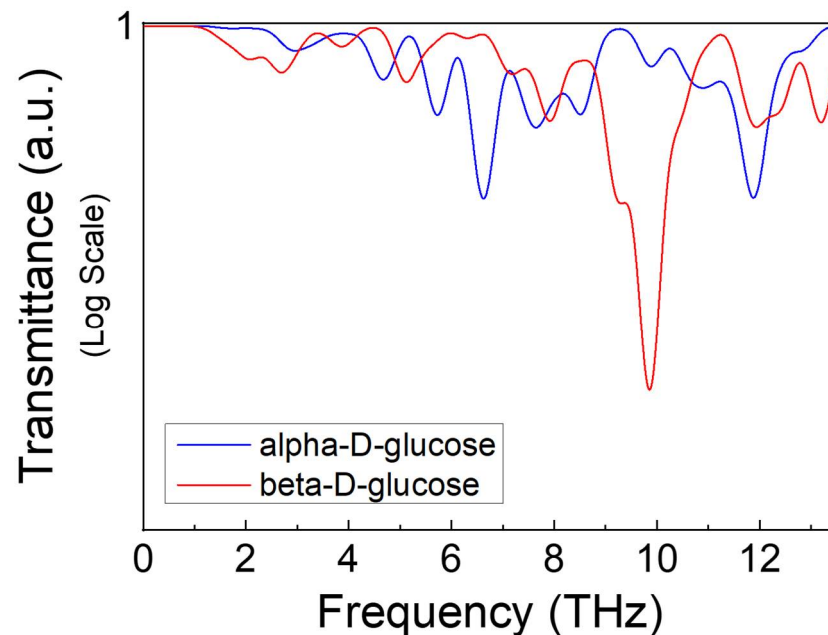


Figure 2. Theoretical transmittance spectra of α - and β -D-glucose crystals. The line spectra were Gaussian broadened with a FWHM of 0.5 THz.

β -D-glucose has a strong absorption band at around 10 THz, while absorption peaks in α -D-glucose can be observed at around 6 THz and its corresponding overtone at 12 THz. Conventional THz-TDS methods, which have a relatively narrow spectral bandwidth, would struggle to detect these features and thus differentiate these two types/forms of glucose.

4. Experiments

4.1. α - and β -D-Glucose

α - or β -D-glucose and polypropylene (SD-PPW5) (host material) powders were mixed with a 3:2 mass ratio (60 wt%), and they were pressed to shape a pellet sample with approximately 1 mm thickness and 12 mm in diameter. The α - and β -D-glucose powders were purchased from Sigma Aldrich Chemistry Co., Inc. (CAS No. 492-62-6), Milwaukee, WI, USA and Tokyo Chemical Industry Co., Ltd. (CAS No. 492-61-5) Tokyo, Japan, respectively. As a reference, a pure pellet of the host material was also prepared. Starch and sucrose exist in large amounts in natural plants, and they are formed of a α -D-glucose polymer and linear condensation of β -D-glucose, thus, non-destructive identification of α - and β -D-glucoses is of great interest in food science and biology. Figure 3a shows the experimentally obtained THz spectra of α - and β -D-glucoses (with each plot being the average of 10 scans) at a frequency step resolution of 0.05 THz. As above mentioned, the spectral resolution is approximately 0.12 THz. Figure 3b also shows the measured absorption spectra by using a conventional FTIR method (frequency resolution: $\sim 4\text{ cm}^{-1}$ ($\sim 0.13\text{ THz}$)). There is an adequate consistence between them in the absorption peaks and

depths. However, the FTIR is still difficult to assign accurately the absorption peaks at 8–10 THz, owing to its low S/N ratio (most 10^{-3}). The α -D-glucose sample exhibited absorption features at 6 and 12 THz, while the β -D-glucose sample exhibited absorption at around 10 THz (Figure 3). Our system allows the full assignment of the absorption peaks predicted by the DFT calculations in the entire THz frequency region.

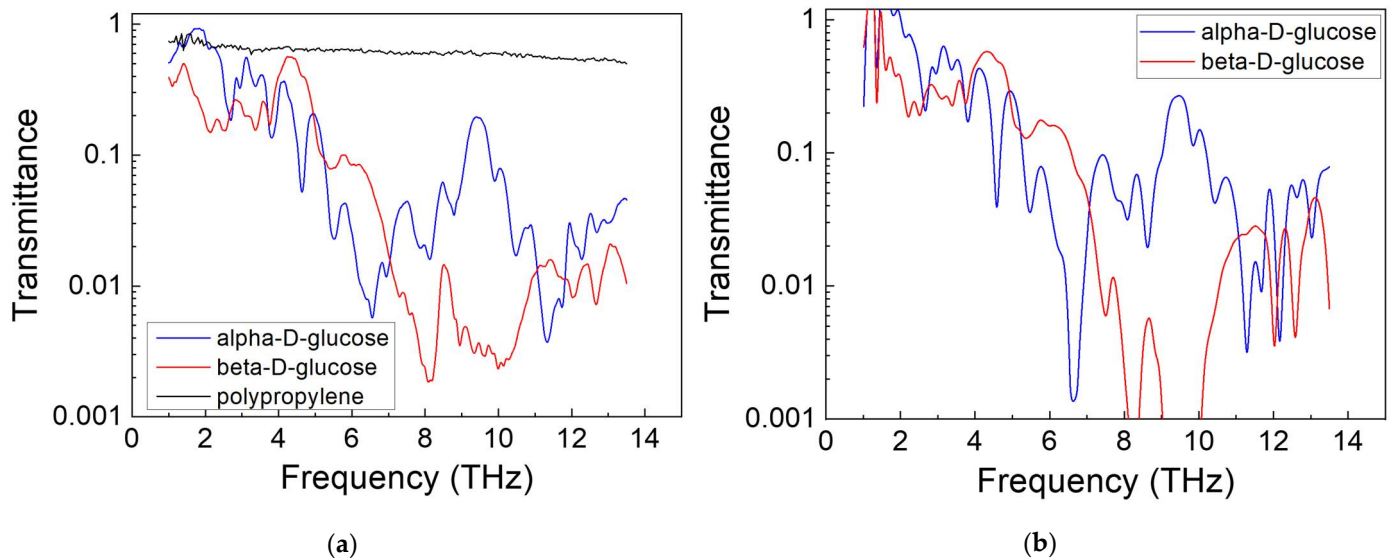


Figure 3. (a) Plots of the experimentally obtained THz transmission characteristics of α - and β -D-glucose and host material of polypropylene samples, characterized using our frequency-domain THz spectroscopic system. (b) THz transmission spectra of α - and β -D-glucose samples measured by using the conventional FTIR method.

These results indicate that this spectroscopic system is capable of resolving and assigning the THz spectral features of anomers of glucose, which are nearly identical stereoisomers and differ only in anomeric carbon.

4.2. D- and L-Glucose

The optical isomers, D- and L-glucose used in this work were obtained from Kanto Chemical Co., Inc. (CAS No. 50-99-7) Tokyo, Japan and Tokyo Chemical Industry Co., Ltd. (CAS No. 921-60-8), Tokyo, Japan, respectively. It should be noted that D-glucose is a naturally occurring substance, while L-glucose is artificially synthesized. Both glucoses should in theory exhibit identical THz absorption characteristics, however, this was not observed in this work. In this work, it was found that L-glucose exhibited a strong absorption feature at 10 THz, which was not observed in D-glucose, as shown in Figure 4. This absorption feature in L-glucose arises from the presence of β -form glucose. As mentioned above, the FTIR was difficult to assign several absorption peaks below a few percent transmission.

We observed that a fabricated sample, made of α - and β -D-glucoses with a mixing ratio of 1:1, exhibited nearly the same absorption characteristics as that of L-glucose (Figure 5). D-glucose, as a naturally occurring substance, has a well-defined molecular form and can clearly be identified using our THz spectroscopy system. L-glucose, on the other hand, is an artificially synthesized substance, which based on our work, typically contains both α - and β -forms. The results demonstrated here, show that our THz spectroscopy system has the potential to identify whether a target material is natural or synthesized.

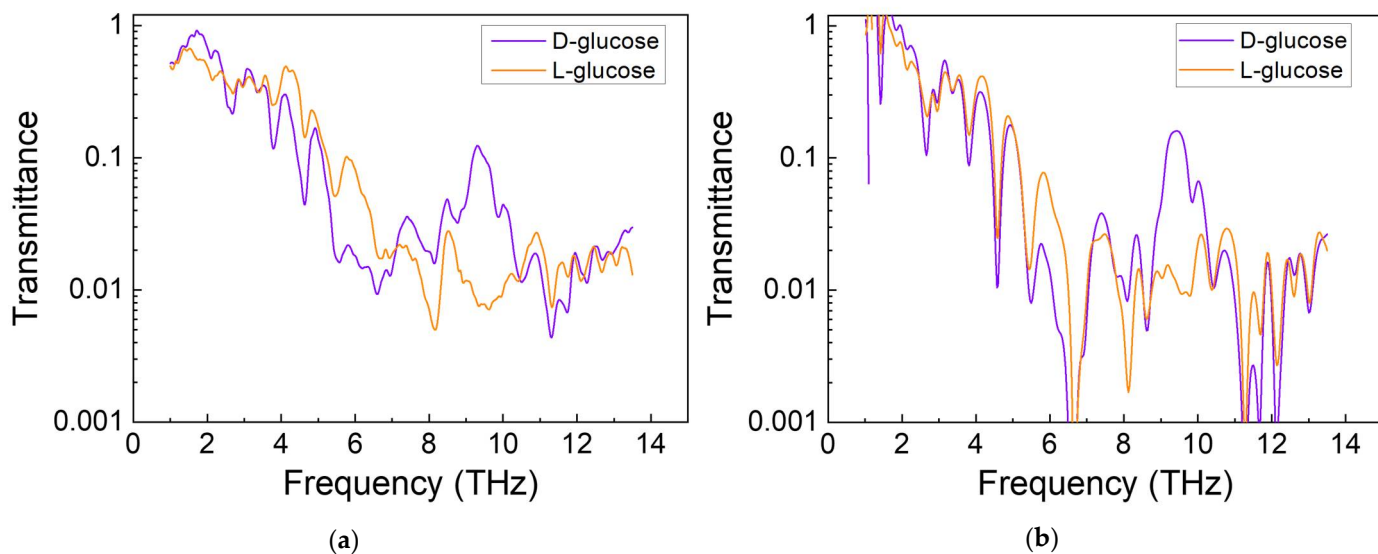


Figure 4. (a) Plots of the experimentally obtained THz transmission characteristics of D- and L-glucose samples, characterized using our frequency-domain THz spectroscopic system. (b) THz transmission spectra of D- and L-glucose samples, measured by the conventional FTIR method.

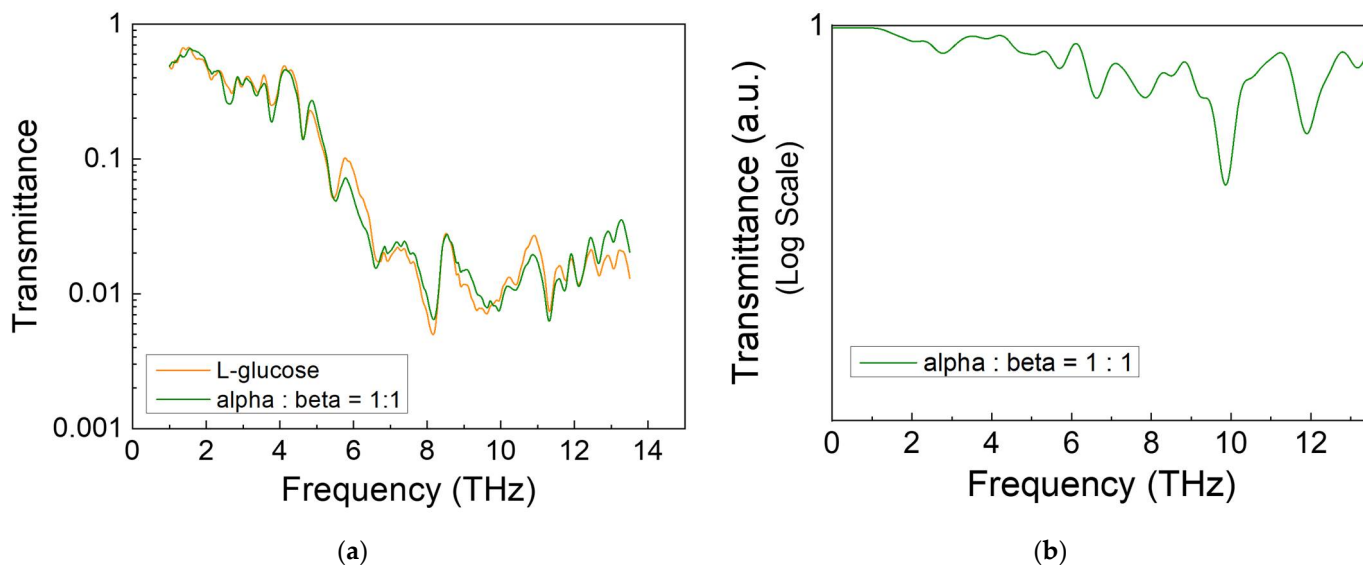


Figure 5. (a) Plots of the experimentally obtained THz transmission characteristics of an L-glucose sample and a mixed sample of α - and β -D-glucose (1:1), obtained using our frequency-domain THz spectroscopic system. (b) Plot of a DFT simulation showing the THz transmittance characteristics of a mixed sample of α - and β -D-glucose with a mixing ratio of 1:1 over a frequency range of 1–13 THz.

5. Conclusions

We have demonstrated the application of an ultrawideband frequency-domain, high-resolution THz spectroscopy system to the differentiation and identification of a range of glucose microcrystals. The results are highlighted by the fact that the THz spectroscopy system operates over a very broad THz frequency range with a signal-to-noise ratio, which far-exceeds that of conventional TDS and FTIR systems. We believe that these characteristics may make it the ideal tool for the identification of a broad range of biological materials and may also be used to differentiate whether substances are natural or artificially synthesized.

Author Contributions: Conceptualization, K.M.; methodology, K.M. and T.O.; software, T.Y., S.T., G.P. and P.K.; validation, K.M., T.Y. and T.O.; formal analysis, G.P. and P.K.; investigation, K.M., T.Y., S.T., K.I., H.U. and A.M.; resources, K.M. and T.O.; data curation, K.M., T.Y., S.T., K.I., H.U., A.M., G.P. and P.K.; writing—original draft preparation, K.M.; writing—review and editing, K.M., H.U., A.M., P.K. and T.O.; visualization, K.M., T.Y., S.T. and K.I.; supervision, K.M.; project administration, K.M.; funding acquisition, K.M., T.O. All authors have read and agreed to the published version of the manuscript.

Funding: This research was partially supported by the Japan Society for the Promotion of Science KAKENHI, grant numbers JP22H01980, JP18H03884, JP22H05131, and JST, CREST Grant Number JPMJCR1903.

Institutional Review Board Statement: Not applicable.

Informed Consent Statement: Not applicable.

Data Availability Statement: Raw data that support the findings of this study are available from the corresponding author upon reasonable request.

Acknowledgments: We acknowledge fruitful discussions and technical support from Seigo Ohno of Tohoku University, and Asako Tsukamoto of Chiba University, respectively.

Conflicts of Interest: The authors declare no conflict of interest.

References

1. Tonouchi, M. Cutting-Edge Terahertz Technology. *Nat. Photonics* **2007**, *1*, 97–105. [[CrossRef](#)]
2. Mittleman, D.M. Twenty Years of Terahertz Imaging [Invited]. *Opt. Express* **2018**, *26*, 9417–9431. [[CrossRef](#)]
3. Dhillon, S.S.; Vitiello, M.S.; Linfield, E.H.; Davies, A.G.; Hoffmann, M.C.; Booske, J.; Paoloni, C.; Gensch, M.; Weightman, P.; Williams, G.P.; et al. The 2017 Terahertz Science and Technology Roadmap. *J. Phys. D* **2017**, *50*, 043001. [[CrossRef](#)]
4. Kiwa, T.; Tonouchi, M.; Yamashita, M.; Kawase, K. Laser Terahertz-Emission Microscope for Inspecting Electrical Faults in Integrated Circuits. *Opt. Lett.* **2003**, *28*, 2058–2060. [[CrossRef](#)]
5. Khalatpour, A.; Paulsen, A.K.; Deimert, C.; Wasilewski, Z.R.; Hu, Q. High-Power Portable Terahertz Laser Systems. *Nat. Photonics* **2021**, *15*, 16–20. [[CrossRef](#)]
6. Nawata, K.; Tokizane, Y.; Takida, Y.; Minamide, H. Tunable Backward Terahertz-Wave Parametric Oscillation. *Sci. Rep.* **2019**, *9*, 726. [[CrossRef](#)]
7. Miyamoto, K.; Sano, K.; Miyakawa, T.; Niinomi, H.; Toyoda, K.; Vallés, A.; Omatsu, T. Generation of High-Quality Terahertz OAM Mode Based on Soft-Aperture Difference Frequency Generation. *Opt. Express* **2019**, *27*, 31840. [[CrossRef](#)]
8. Miyamoto, K.; Nomura, R.; Tsurumaru, S.; Omatsu, T. Tunable Terahertz Bessel Beams with Orbital Angular Momentum. *Opt. Contin.* **2022**, *1*, 633. [[CrossRef](#)]
9. Hirori, H.; Shinokita, K.; Shirai, M.; Tani, S.; Kadoya, Y.; Tanaka, K. Extraordinary Carrier Multiplication Gated by a Picosecond Electric Field Pulse. *Nat. Commun.* **2011**, *2*, 594–596. [[CrossRef](#)]
10. Tanaka, K.; Hirori, H.; Nagai, M. THz Nonlinear Spectroscopy of Solids. *IEEE Trans. Terahertz Sci. Technol.* **2011**, *1*, 301–312. [[CrossRef](#)]
11. Nagai, M.; Aono, S.; Ashida, M.; Kawase, K.; Irizawa, A.; Isoyama, G. Luminescence Induced by Electrons Outside Zinc Oxide Nanoparticles Driven by Intense Terahertz Pulse Trains. *New J. Phys.* **2017**, *19*, 053017. [[CrossRef](#)]
12. Tani, S.; Blanchard, F.; Tanaka, K. Ultrafast Carrier Dynamics in Graphene under a High Electric Field. *Phys. Rev. Lett.* **2012**, *109*, 166603. [[CrossRef](#)]
13. Sie, E.J.; Nyby, C.M.; Pemmaraju, C.D.; Park, S.J.; Shen, X.; Yang, J.; Hoffmann, M.C.; Ofori-Okai, B.K.; Li, R.; Reid, A.H.; et al. An Ultrafast Symmetry Switch in a Weyl Semimetal. *Nature* **2019**, *565*, 61–66. [[CrossRef](#)]
14. Luo, L.; Yang, X.; Liu, X.; Liu, Z.; Vaswani, C.; Cheng, D.; Mootz, M.; Zhao, X.; Yao, Y.; Wang, C.Z.; et al. Ultrafast Manipulation of Topologically Enhanced Surface Transport Driven by Mid-Infrared and Terahertz Pulses in Bi₂Se₃. *Nat. Commun.* **2019**, *10*, 607. [[CrossRef](#)]
15. Arikawa, T.; Hiraoka, T.; Morimoto, S.; Blanchard, F.; Tani, S.; Tanaka, T.; Sakai, K.; Kitajima, H.; Sasaki, K.; Tanaka, K. Transfer of Orbital Angular Momentum of Light to Plasmonic Excitations in Metamaterials. *Sci. Adv.* **2020**, *6*, eaay1977. [[CrossRef](#)]
16. Yoshikawa, N.; Tamaya, T.; Tanaka, K. High-Harmonic Generation in Graphene Enhanced by Elliptically Polarized Light Excitation. *Science (1979)* **2017**, *356*, 736–738. [[CrossRef](#)]
17. Kovalev, S.; Dantas, R.M.A.; Germanskiy, S.; Deinert, J.C.; Green, B.; Ilyakov, I.; Awari, N.; Chen, M.; Bawatna, M.; Ling, J.; et al. Non-Perturbative Terahertz High-Harmonic Generation in the Three-Dimensional Dirac Semimetal Cd₃As₂. *Nat. Commun.* **2020**, *11*, 6–11. [[CrossRef](#)]
18. Miyamoto, K.; Kang, B.J.; Kim, W.T.; Sasaki, Y.; Niinomi, H.; Suizu, K.; Rotermund, F.; Omatsu, T. Highly Intense Monocycle Terahertz Vortex Generation by Utilizing a Tsurupica Spiral Phase Plate. *Sci. Rep.* **2016**, *6*, 38880. [[CrossRef](#)]

19. Yamazaki, S.; Harata, M.; Ueno, Y.; Tsubouchi, M.; Konagaya, K.; Ogawa, Y.; Isoyama, G.; Otani, C.; Hoshina, H. Propagation of THz Irradiation Energy through Aqueous Layers: Demolition of Actin Filaments in Living Cells. *Sci. Rep.* **2020**, *19*, 9008. [[CrossRef](#)]
20. Hsieh, Y.D.; Iyonaga, Y.; Sakaguchi, Y.; Yokoyama, S.; Inaba, H.; Minoshima, K.; Hindle, F.; Araki, T.; Yasui, T. Spectrally Interleaved, Comb-Mode-Resolved Spectroscopy Using Swept Dual Terahertz Combs. *Sci. Rep.* **2014**, *4*, 3816. [[CrossRef](#)]
21. Kutas, M.; Haase, B.; Bickert, P.; Riexinger, F.; Molter, D.; von Freymann, G. Terahertz Quantum Sensing. *Sci. Adv.* **2020**, *6*, eaaz8065. [[CrossRef](#)] [[PubMed](#)]
22. Cocker, T.L.; Jelic, V.; Hillenbrand, R.; Hegmann, F.A. Nanoscale Terahertz Scanning Probe Microscopy. *Nat. Photonics* **2021**, *15*, 558–569. [[CrossRef](#)]
23. Matsumoto, H.; Watanabe, I.; Kasamatsu, A.; Monnai, Y. Integrated Terahertz Radar Based on Leaky-Wave Coherence Tomography. *Nat. Electron.* **2020**, *3*, 122–129. [[CrossRef](#)]
24. Valušis, G.; LISAUSKAS, A.; Yuan, H.; Knap, W.; Roskos, H.G. Roadmap of Terahertz Imaging 2021. *Sensors* **2021**, *21*, 4092. [[CrossRef](#)] [[PubMed](#)]
25. Vallés, A.; He, J.; Ohno, S.; Omatsu, T.; Miyamoto, K. Broadband High-Resolution Terahertz Single-Pixel Imaging. *Opt. Express* **2020**, *28*, 28868–28881. [[CrossRef](#)] [[PubMed](#)]
26. Kiwa, T.; Akiwa, Y.; Fujita, H.; Teranishi, T.; Sakai, K.; Nose, H.; Kobayashi, M.; Tsukada, K. Electric Potential Distribution on Lithium Ion Battery Cathodes Measured Using Terahertz Chemical Microscopy. *J. Infrared Millim. Terahertz Waves* **2020**, *41*, 430–437. [[CrossRef](#)]
27. Shen, Y.C.; Upadhyaya, P.C.; Linfield, E.H.; Davies, A.G. Vibrational Spectra of Nucleosides Studied Using Terahertz Time-Domain Spectroscopy. *Vib. Spectrosc.* **2004**, *35*, 111–114. [[CrossRef](#)]
28. Fischer, B.M.; Walther, M.; Uhd Jepsen, P. Far-Infrared Vibrational Modes of DNA Components Studied by Terahertz Time-Domain Spectroscopy. *Phys. Med. Biol.* **2002**, *47*, 3807–3814. [[CrossRef](#)]
29. Yamaguchi, M.; Miyamaru, F.; Yamamoto, K.; Tani, M.; Hangyo, M. Terahertz Absorption Spectra of L-, D-, and DL-Alanine and Their Application to Determination of Enantiometric Composition. *Appl. Phys. Lett.* **2005**, *86*, 053903. [[CrossRef](#)]
30. Plusquellic, D.F.; Siegrist, K.; Heilweil, E.J.; Esenturk, O. Applications of Terahertz Spectroscopy in Biosystems. *ChemPhysChem* **2007**, *8*, 2412–2431. [[CrossRef](#)]
31. Neu, J.; Stone, E.A.; Spies, J.A.; Storch, G.; Hatano, A.S.; Mercado, B.Q.; Miller, S.J.; Schmuttenmaer, C.A. Terahertz Spectroscopy of Tetrameric Peptides. *J. Phys. Chem. Lett.* **2019**, *10*, 2624–2628. [[CrossRef](#)] [[PubMed](#)]
32. Spies, J.A.; Neu, J.; Tayvah, U.T.; Capobianco, M.D.; Pattengale, B.; Ostresh, S.; Schmuttenmaer, C.A. Terahertz Spectroscopy of Emerging Materials. *J. Phys. Chem. C* **2020**, *124*, 22335–22346. [[CrossRef](#)]
33. Laman, N.; Harsha, S.S.; Grischkowsky, D.; Melinger, J.S. High-Resolution Waveguide THz Spectroscopy of Biological Molecules. *Biophys. J.* **2008**, *94*, 1010–1020. [[CrossRef](#)]
34. Jeong, K.; Huh, Y.-M.; Kim, S.-H.; Park, Y.; Son, J.-H.; Oh, S.J.; Suh, J.-S. Characterization of Blood Using Terahertz Waves. *J. Biomed. Opt.* **2013**, *18*, 107008. [[CrossRef](#)] [[PubMed](#)]
35. Chen, H.; Chen, X.; Ma, S.; Wu, X.; Yang, W.; Zhang, W.; Li, X. Quantify Glucose Level in Freshly Diabetic's Blood by Terahertz Time-Domain Spectroscopy. *J. Infrared Millim. Terahertz Waves* **2018**, *39*, 399–408. [[CrossRef](#)]
36. Koichi, M.; Miyamoto, K.; Ujita, S.; Saito, T.; Ito, H.; Omatsu, T. Dual-Frequency Picosecond Optical Parametric Generator Pumped by a Nd-Doped Vanadate Bounce Laser. *Opt. Express* **2011**, *19*, 18523–18528. [[CrossRef](#)]
37. Kawase, K.; Mizuno, M.; Sohma, S.; Takahashi, H.; Taniuchi, T.; Urata, Y.; Wada, S.; Tashiro, H.; Ito, H. Difference-Frequency Terahertz-Wave Generation from 4-Dimethylamino-N-Methyl-4'-Stilbazolium-Tosylate by Use of an Electronically Tuned Ti:Sapphire Laser. *Opt. Lett.* **1999**, *24*, 1065–1067. [[CrossRef](#)]
38. Uchida, H.; Oota, K.; Minami, T.; Takeya, K.; Kawase, K. Generation of Single-Cycle Terahertz Pulse Using Cherenkov Phase Matching with 4-Dimethylamino-N'-Methyl-4'-Stilbazolium Tosylate Crystal. *Appl. Phys. Express* **2017**, *10*, 062601. [[CrossRef](#)]
39. Ohno, S.; Miyamoto, K.; Minamide, H.; Ito, H. New Method to Determine the Refractive Index and the Absorption Coefficient of Organic Nonlinear Crystals in the Ultra-Wideband THz Region. *Opt. Express* **2010**, *18*, 17306–17312. [[CrossRef](#)]
40. He, Y.; Wang, Y.; Xu, D.; Nie, M.; Yan, C.; Tang, L.; Shi, J.; Feng, J.; Yan, D.; Liu, H.; et al. High-Energy and Ultra-Wideband Tunable Terahertz Source with DAST Crystal via Difference Frequency Generation. *Appl. Phys. B Lasers Opt.* **2018**, *124*, 16. [[CrossRef](#)]
41. Kresse, G.; Furthmüller, J. Efficient Iterative Schemes for Ab Initio Total-Energy Calculations Using a Plane-Wave Basis Set. *Phys. Rev. B* **1996**, *54*, 11169. [[CrossRef](#)]
42. Debbichi, L.; Marco De Lucas, M.C.; Pierson, J.F.; Krüger, P. Vibrational Properties of CuO and Cu₄O₃ from First-Principles Calculations, and Raman and Infrared Spectroscopy. *J. Phys. Chem. C* **2012**, *116*, 10232–10237. [[CrossRef](#)]
43. Brown, G.M.; Levy, H.A. α -D-Glucose: Precise Determination of Crystal and Molecular Structure by Neutron-Diffraction Analysis. *Science (1979)* **1965**, *147*, 1038–1039. [[CrossRef](#)]
44. Chu, S.S.C.; Jeffrey, G.A. IUCr The Refinement of the Crystal Structures of β -d-Glucose and Cellobiose. *Acta Cryst.* **1968**, *24*, 830–838. [[CrossRef](#)]
45. Gajdoš, M.; Hummer, K.; Kresse, G.; Furthmüller, J.; Bechstedt, F. Linear Optical Properties in the Projector-Augmented Wave Methodology. *Phys. Rev. B—Condens. Matter Mater. Phys.* **2006**, *73*, 045112. [[CrossRef](#)]